Elastic scattering and ^{7}Li production in the ^{8}Li + ^{120}Sn reaction

O. C. B. Santos [*], R. Lichtenthäler Filho [†], K. C. C. Pires, U. Umbelino, E. O. N. Zevallos [‡], A. L. de Lara,
A. S. Serra, V. Scarduelli, J. Alcántara-Núñez, and A. Lépine-Szily

Departamento de Física Nuclear, Instituto de Física, Universidade de São Paulo, 05508-090 São Paulo, Brazil

A. M. Moro

Departamento de Física Atómica, Molecular y Nuclear, Facultad de Física, Universidad de Sevilla, Apartado 1065, E-41080 Sevilla, Spain

S. Appannababu

Department of Nuclear Physics, Andhra University, Visakhapatnam 530 003, India

M. Assunção

Departamento de Física, Universidade Federal de São Paulo, UNIFESP, 09913-030 Diadema, Brazil

Jin Lei

School of Physics Science and Engineering, Tongji University, Shanghai 200092, China

The ^{8}Li + ^{120}Sn collision has been investigated at laboratory energies of 21.7 and 25.8 MeV ($V_{CB}^{lab} =$ 20.5 MeV). The ^{8}Li + ^{120}Sn elastic scattering and the ^{7}Li fragment angular and energy distributions from the ^{120}Sn(^{8}Li, ^{7}Li)X reaction have been measured. The elastic scattering angular distributions were analyzed by optical model and coupled reaction channels (CRC) calculations considering the coupling with the neutron stripping channel. The effect of the projectile breakup on the elastic scattering distributions has been studied via continuum-discretized coupled-channels (CDCC) calculations. The experimental ^{7}Li energy distribution presents characteristics similar to a neutron transfer reaction populating a wide range of excited states in the recoil system, from the ground state up to states above the neutron threshold, with a maximum in the excitation energy predicted by Q-optimum arguments. These energy distributions, as well as the corresponding ^{7}Li angular distributions, are well described using the Ichimura, Austern, and Vincent (IAV) model, which includes the neutron transfer to bound and unbound states of the target nucleus. The total reaction cross sections from the elastic scattering angular distributions and total breakup cross sections have been obtained from the IAV plus CDCC and CRC calculations. A comparison with previous measurements of the ^{8}Li scattering on ^{9}Be and ^{58}Ni targets is presented. A dominance of the transfer to bound states over the breakup channel is seen in the present case.

I. INTRODUCTION

In recent years, low energy measurements have been performed of the elastic scattering, transfer and breakup reactions of light unstable and exotic projectiles on different mass targets [1–21]. Collisions induced by projectiles with alpha structure such as ^{6}He and ^{6}Li [22–31] show a large production of alpha particles which, in many cases, is not reproduced by continuum discretized coupled channels (CDCC) calculations. Although ^{8}Li cannot be considered an exotic nucleus, its small $1n$ separation threshold of 2.03 MeV makes it an interesting case. A review of elastic scattering and reactions of light exotic beams, including the ^{8}Li case, is presented in

Ref. [1]. More recently, measurements with the ^{8}Li projectile have been performed on ^{58}Ni and ^{9}Be targets [2,3]. In both cases, a large production of ^{7}Li particles has been reported, presenting a wide energy distribution around the ^{8}Li scattered peak. Inspection of the ^{7}Li energy distribution indicates that these particles are fragments of the projectile, produced in reactions corresponding to the population of highly excited states of the recoil system (target+neutron). The fragment Q-value distributions are centered close to the expected transfer Q-optimum (Q_{opt}) value which, for neutron transfer, lies around $Q \approx 0$ [32]. The experimental width of the fragment energy distributions is about 4–5 MeV. The fact that momentum matching conditions favor transfer with $Q \approx 0$ for neutrons implies that the difference between the binding energies of the transferred neutron in the projectile (entrance channel) and in the target (exit channel) should be also around zero. As a consequence, neutron transfer reactions induced by

---

[*]Contact author: osvaldo.santos@usp.br

[†]Contact author: rubens@if.usp.br

[‡]Present address: Universidad Científica del Sur, Lima 15067, Peru.

weakly bound and exotic projectiles will preferably populate weakly bound states in the final nucleus, close to the neutron separation threshold.

In a typical inclusive breakup measurement, in which only one of the fragments resulting from the projectile is detected (the ^{7}Li system in the present case), the data will contain in general contributions coming from the population of final states of the neutron+target residual system above and below the neutron breakup threshold. Although the latter corresponds strictly to transfer in the usual sense, it has become customary to refer to all these processes globally as *inclusive breakup reactions*. Furthermore, for transitions above the neutron breakup threshold, a convenient separation is made between the so-called *elastic breakup* (EBU) and the *nonelastic breakup* (NEB) components, distinguishing the cases in which the target remains in its ground state EBU from those which involve some kind of excitation of the target or some rearrangement between the unobserved projectile fragments and the target system. Existing state-of-the-art reaction formalisms permit a separate evaluation of the EBU and NEB contributions. The EBU component can be accurately obtained with the CDCC method, while the NEB part can be estimated using the formalism developed by Ichimura, Austern, and Vincent (IAV) [33].

In this paper, we present new data for the ^{8}Li + ^{120}Sn collision and compare the present measurements with previously obtained total breakup cross sections for ^{8}Li projectile on ^{9}Be and ^{58}Ni targets.

One of the motivations of the present work is the investigation of the origin of the large observed ^{7}Li yields. For that, CDCC and IAV calculations will be performed and compared with the data. The angle-integrated breakup cross sections will be compared with those from other ^{8}Li-induced reactions.

The paper is organized as follows. In Sec. II we describe the experimental setup of the experiment. In Sec. III we present a theoretical analysis of the elastic and inclusive breakup data, including CDCC, IAV, and coupled reaction channels (CRC) calculations. Finally, in Sec. IV we summarize the main results of this work.

II. EXPERIMENTAL SETUP

The experiment was performed at the Radioactive Ion Beams in Brazil (RIBRAS) system [34–39], installed at the 8-UD tandem accelerator at the University of São Paulo in a way similar to that described for the ^{8}Li + ^{58}Ni and ^{8}Li + ^{9}Be systems in previous papers [2,3]. The ^{8}Li secondary beams were produced by the ^{9}Be(^{7}Li, ^{8}Li)^{8}Be transfer reaction, utilizing ^{7}Li primary beams at two energies $E_{lab} = 28$ and 24 MeV with $I_{beam} = 300$ nA e, delivered by the 8-UD Pelletron. The ^{8}Li secondary beams were selected and focused by the first solenoid in the center of the ISO-250 scattering chamber located between the two solenoids. Four ΔE-E silicon telescopes were used to detect and identify the scattered particles. The detectors have an active area of 150 mm^2 with thicknesses of 25 and 1000 μm for the ΔE and E detectors, respectively. Secondary targets of ^{197}Au and ^{120}Sn, with thicknesses of 4 mg/cm^2, were mounted in the center of the scattering chamber. The pure Rutherford ^{8}Li + ^{197}Au scattering is used

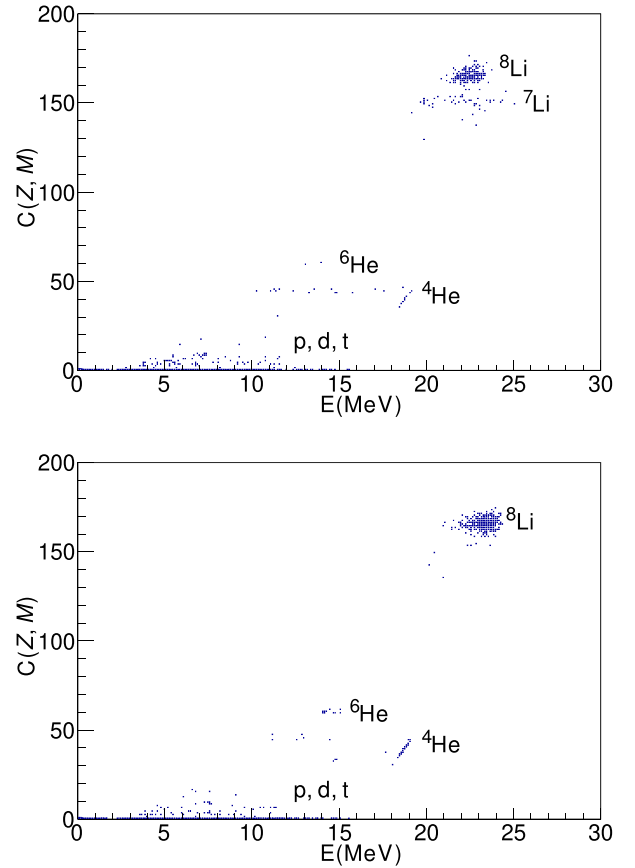FIG. 1. Two-dimensional $C(Z, M)$-E identification spectra obtained with ^{120}Sn (top) and gold (bottom) targets at $\theta_{lab} = 69°$ and an incident energy of 25.8 MeV for ^{8}Li.

to monitor the secondary beam and to normalize the cross sections.

Two-dimensional $C(Z, M)$-E spectra obtained with tin and gold targets for the energy of 25.8 MeV are presented in Fig. 1. The quantity $C(Z, M)$ is defined as $C(Z, M) = (E)^b - (E - \Delta E)^b$ with $E = E_{\text{Residual}} + \Delta E$ [40], where E_{Residual} and ΔE are the signals from the telescopes and $b = 1.6$ was adjusted. This method provides a (Z, M) identification of the particles. We clearly see that the ^{8}Li peak is well separated from the lighter ^{4,6}He, p, d, t contaminants.

In the upper part of Fig. 1, corresponding to the tin target, one sees the presence of ^{7}Li events just below the ^{8}Li peak. Those events are not present in the gold target measurements (lower graph), indicating that the ^{7}Li particles have been produced in reactions with the tin target.

The ^{8}Li + ^{120}Sn elastic scattering angular distributions at 21.7 and 25.8 MeV bombarding energies are presented in Fig. 2. Only the statistical errors were taken into account in the experimental data.

The ^{7}Li energy distribution at 25.8 MeV is presented in Fig. 3 and the energy-integrated ^{7}Li angular distributions measured at both bombarding energies are shown in Fig. 4.

In Fig. 3, we plot the ^{7}Li energy distribution as a function of the reaction Q-value, using the two-body ^{120}Sn(^{8}Li, ^{7}Li)^{121}Sn* reaction kinematics to transform
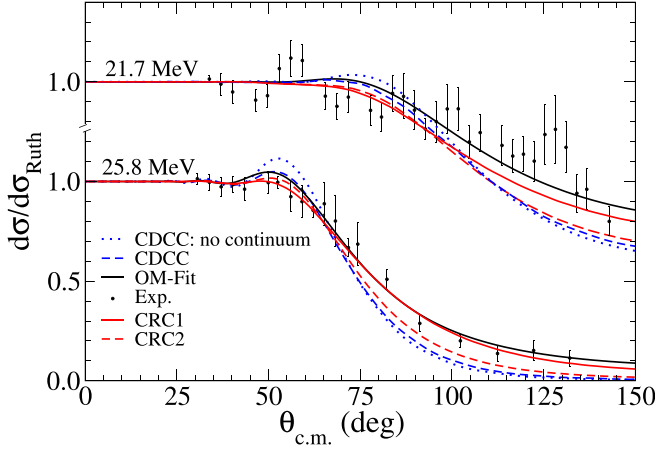
FIG. 2. ^{8}Li + ^{120}Sn experimental elastic scattering angular distributions compared with the CDCC no-continuum (dotted blue line), full CDCC (dashed blue line), CRC (solid and dashed red lines), and OM-Fit (solid black line).

$E_{^7Li} \rightarrow Q$, in the same way as previously done in the ^{9}Be and ^{58}Ni analysis [2,3]. This transformation allows us to sum the ^{7}Li yields for different scattering angles in the same spectrum, improving the statistics. In the upper horizontal axis of Fig. 3 we show the corresponding excitation energy of the $n + {}^{120}$Sn recoil system. The ^{7}Li energy distribution at 21.7 MeV is omitted due to poorer statistics.

Phenomenological discussion of the experimental results

It is clear from Fig. 3, that the energy distribution presents a maximum around $Q \approx 0$ as expected from momentum matching considerations for neutron transfer reactions. A value of Q_{opt} somewhat lower than zero is possible due to the angular
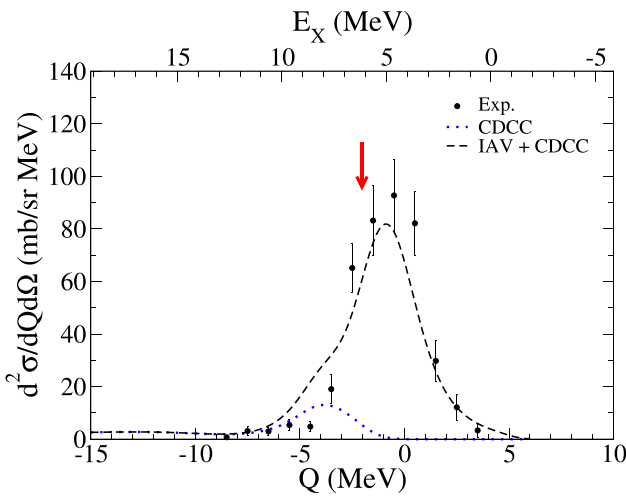

FIG. 3. Experimental Q-value distribution for ^{120}Sn(^{8}Li, ^{7}Li)X reaction compared to IAV+CDCC calculations (solid black line) and CDCC (dotted blue line). In the upper horizontal axis we show the corresponding excitation energy of the recoil X system. The red arrow separates bound (right) and unbound (left) states in the $n + {}^{120}$Sn excited system.

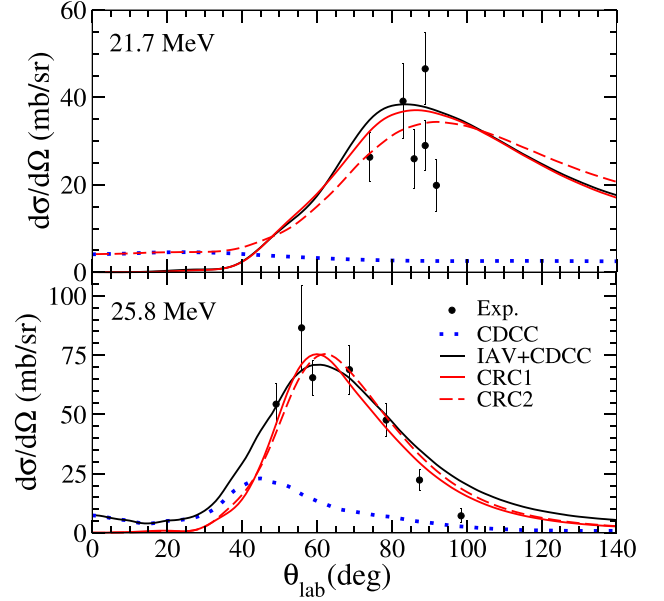FIG. 4. Experimental ^{7}Li angular distribution compared with IAV+CDCC calculations (solid black line), CDCC (dotted blue line), and CRC (solid and dashed red line).

momentum transferred in the reaction [25,32]. We also see, in the upper horizontal (excitation energy) axis of Fig. 3, that the reaction populates states around 5 MeV excitation energy, just below the 6.170 MeV neutron threshold of ^{121}Sn (see red arrow). The red arrow in Fig. 3 indicates the neutron emission threshold, which separates bound (right) and unbound (left) states in the ^{121}Sn recoil nucleus. One sees that most of the cross section lies in the region of bound states, indicating that neutron stripping dominates in the present ^{8}Li + ^{120}Sn data, which contrasts to the previously analyzed ^{58}Ni [3] and ^{9}Be [2] cases, where contributions from bound and unbound states were similar.

The ^{7}Li angular distributions presented in Fig. 4 present maxima at around 85° and 60° for 21.7 and 25.8 MeV, respectively. Those angles would correspond to approximately 88° and 63° in the center-of-mass (CM) frame assuming the ^{120}Sn(^{8}Li, ^{7}Li) ^{121}Sn kinematics with $Q = 0$. Those grazing angles are considerably smaller than the $\theta_{1/4}$ angles obtained from the elastic scattering angular distributions (see Fig. 2), indicating that the transfer reaction takes place at partial waves larger than the usual grazing angular momentum obtained from the elastic scattering.

III. THEORETICAL ANALYSIS

In the present section, we will present a detailed analysis of the data, including the ^{8}Li + ^{120}Sn elastic scattering angular distributions and the ^{7}Li energy and angular distributions at the two measured energies. First, we performed optical model (OM) calculations to obtain appropriate OM potentials for the entrance channel. Next, we compared the elastic distributions with CDCC and coupled-channels (CC) calculations. It is worth noticing that the measured ^{8}Li + ^{120}Sn elastic angular distributions are indeed quasielastic, as we are unable to

separate possible contributions from the excitation of low-lying states of the projectile and target due to our experimental energy resolution. However, we performed detailed coupled-channels calculations to estimate the effect of the projectile and target excitations on the "elastic" angular distributions, using known values of $B(E2)$ and nuclear deformations for ^{120}Sn and ^{8}Li. In all cases, we found that the effect of inelastic scattering is negligible in the entire angular range of our measurements, so that from now on we will refer to the ^{8}Li + ^{120}Sn distributions as purely elastic.

Finally, we compared the measured inclusive ^{7}Li distributions with calculations based on the IAV and CRC formalisms, and we will discuss the effect of the neutron stripping channel on the elastic cross sections.

A. Optical model

As a first step in the analysis of the elastic scattering angular distributions, an optical model calculation was performed, using FRESCO code [41]. We used a double-folding (DF) as bare potential, obtained by convoluting the M3Y nucleon-nucleon interaction with the ^{8}Li ground-state density from Ref. [42]. The real and imaginary potentials were renormalized to $N_r = N_i = 0.6$. The need for the use of reduced normalizations in the folding potentials for weakly bound projectiles has long been recognized [43–49]. More recently, CDCC calculations for weakly bound and exotic projectiles suggest that the projectile breakup and transfer reactions generate a repulsive term in the real part of the dynamic polarization polarization potential which could be accounted for by a smaller normalization in the real part of the folded potential [50–52]. Additionally, an imaginary Woods-Saxon surface derivative term was added to the DF bare potential, and its parameters were adjusted to optimize the fit to experimental data. The following fitting parameters were obtained: $W_d = 25.0$ MeV, $r_w = 1.30$ fm, and $a_w = 0.39$ fm, with $R = r_i(A_T^{1/3} + A_p^{1/3})$. The result of this fit is shown in Fig. 2 as the black solid line. The same potential parameters were used for both energies.

The DF bare potential with $N_r = N_i = 0.6$ without the surface derivative term will be used as bare potential in the CRC calculations, to be presented in the further sections.

B. Effect of the projectile breakup on the elastic scattering

The projectile elastic breakup contribution was calculated with the CDCC framework, using a two-body model (^{7}Li + n) of the ^{8}Li nucleus. For the CDCC calculation we used FRESCO code [41]. These calculations require optical potentials for the fragment+target systems. For the ^{7}Li + ^{120}Sn system, an energy-dependent Woods-Saxon optical potential was derived using experimental data from the literature [53,54] at several incident energies, with final parameters $V = (382.7 + 4.691E)$ MeV, $r_v = 1.386$ fm, $a_v = 0.60$ fm, $W = 14.6$ MeV, $r_w = 1.65$ fm, $a_w = 0.759$ fm, and $r_c = 1.3$ fm, with $R_i = r_i A^{1/3}$. For the $n + ^{120}$Sn system, the global potential of Koning and Delaroche (KD) was used [55]. All these potentials are energy dependent, but, in the present CDCC calculations, they are evaluated at the same energy per nucleon as the

incident projectile. The energy dependence will be relevant for the IAV calculations presented in Sec. III C. The continuum states were discretized considering a maximum orbital angular momentum of $l_{max} = 3$ and energy bins with a maximum energy of $\epsilon_{max} = 7.2$ MeV. In these conditions, convergence of the CDCC calculation was attained in the elastic scattering channel.

The results are shown in Fig. 2. The dotted blue line corresponds to the no continuum CDCC calculation and the dashed blue line is the full CDCC calculation, including the projectile breakup effect. It is observed that the reduction of the Fresnel peak, observed at forward angles, is partially explained by the coupling with the projectile breakup channel; however, the cross sections at angles larger than $70°$ for the energy of 25.8 MeV and $95°$ for the energy of 21.7 MeV are underestimated by the CDCC calculation.

C. Inclusive transfer/breakup contributions

The nonelastic breakup contributions to the total inclusive breakup cross section have been estimated with the IAV model [33]. This model was recently applied to a variety of reactions induced by stable and unstable weakly bound projectiles, providing in general good agreement with existing data [2,3,56–59]. The IAV method relies on the distorted-wave Born approximation (DWBA) of the breakup transition amplitude for the reaction ^{8}Li + ^{120}Sn $\rightarrow$ ^{7}Li + X, where X represents any possible final state of the $n + ^{120}$Sn system. The main ingredients of these calculations are the interactions for the ^{7}Li + ^{120}Sn, ^{7}Li + ^{121}Sn, and $n + ^{120}$Sn systems, which are approximated by suitable energy-dependent optical potentials, as described in Sec. III B. For the entrance channel (^{8}Li + ^{120}Sn), the optical potential obtained in Sec. III A was used. Note that the model accounts for the inclusive breakup comprising the transfer to continuum (TC) as well as the transfer to bound states contribution, which is naturally obtained in this formalism by extrapolation of the $n + ^{120}$Sn optical potential at negative neutron energies.

The results of the calculations are shown in Figs. 3 and 4 where in each figure the dotted line is the EBU contribution, calculated with CDCC, and the solid black line is the sum of the EBU and NEB contributions, the latter computed with IAV. As one can see, an excellent agreement is obtained for both the ^{7}Li energy and the angular distributions. Furthermore, it is apparent that the elastic breakup contributes very little to the inclusive ^{7}Li production; in fact, most of the ^{7}Li yield comes from the neutron transfer channel to bound states, but also to continuum states (TC).

D. Coupled reaction channel calculations

In order to investigate the influence of the one-neutron transfer on the elastic scattering, CRC calculations were performed considering the coupling between the elastic and ^{120}Sn(^{8}Li, ^{7}Li) ^{121}Sn* channels, using FRESCO code [41]. The double folding potential with $N_r = N_i = 0.6$, derived in Sec. III A, was used as the bare potential in the next CRC calculations.

TABLE I. Spectroscopic amplitudes, A_{nlj}, considered in the CRC calculations for the overlaps $\langle ^{120}\text{Sn}|^{121}\text{Sn}\rangle$.

nlj	CRC1		CRC2	
	E_x	A_{nlj}	E_x	A_{nlj}
$2d_{3/2}$	0.000	1.000	0.000	0.190
$1h_{11/2}$	0.008	1.000	0.008	0.329
$3s_{1/2}$	0.207	1.000	0.207	0.437
$1g_{7/2}$	0.994	1.000	0.994	0.606
$2d_{5/2}$	1.175	1.000	1.175	0.867
$2f_{7/2}$	2.880	1.000	3.110	1.000
$3p_{3/2}$	3.750	1.000	4.970	1.000
$2f_{5/2}$	5.210	1.000	bin	1.000
$1h_{9/2}$	bin	1.000	bin	1.000
$1i_{13/2}$	bin	1.000	bin	1.000

TABLE II. Spectroscopic amplitudes for the overlaps $\langle ^8\text{Li}|^7\text{Li}\rangle$.

J^π	$J^\pi_{^7\text{Li}}$	nlj	A_{nlj}
2^+	$3/2^-$	$1p_{3/2}$	0.943
	$3/2^-$	$1p_{1/2}$	0.471
	$1/2^-$	$1p_{3/2}$	-0.471
1^+	$3/2^-$	$1p_{1/2}$	0.816
	$1/2^-$	$1p_{3/2}$	0.816
3^+	$3/2^-$	$1p_{3/2}$	0.632

Because the populated states in $^{121}\text{Sn}^*$ span a broad excitation energy range, including bound and unbound states, in a region where the level density is large, it is not feasible to take into account all the accessible physical states in the CRC calculations. Instead, we replace the physical ^{121}Sn states by a set of representative states, one for each nlj configuration, to be considered in the coupling scheme. These states were placed at excitation energies corresponding to the *centers of gravity* of the ^{121}Sn single-particle states, taken from the literature [3,60]. Unbound states were also taken into account in the calculations by including a set of energy bins above the $n + ^{120}\text{Sn}$ threshold (see Table I).

Concerning the $n + ^{120}\text{Sn}$ spectroscopic factors of those representative states, two calculations were performed. In the first one, all the $n + ^{120}\text{Sn}$ spectroscopic factors are taken as unity, which would be consistent with pure single-particle states in the absence of pairing. In the second, spectroscopic factors obtained by a BCS calculation performed with the code HFBCS+QRPA [61,62] with the Skyrme SLy5 interaction (see Table I) were used. This calculation takes into account the partial occupation of the single-particle levels above and below the Fermi surface, which is expected to be a more realistic picture for a superfluid nucleus like ^{120}Sn.
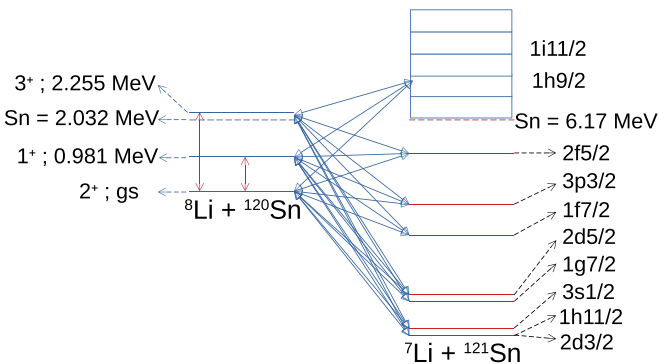
In Fig. 5, we show the coupling scheme used in these calculations. For the entrance channel we used the DF potential described in Sec. III A, and for the $^7\text{Li} + ^{120}\text{Sn}$, $^7\text{Li} + ^{121}\text{Sn}$, and $n + ^{120}\text{Sn}$ systems we used the same potentials described in Sec. III C at the corresponding energy. Unlike the IAV calculations, the $n + ^{120}\text{Sn}$ potential used here is purely real. For bound states, the depth of the real part of the $n + ^{120}\text{Sn}$ potential is adjusted to reproduce the $n + ^{120}\text{Sn}$ separation energy. For the calculations with unit spectroscopic factors, we also included states in the continuum of $n + ^{120}\text{Sn}$ for each representative state. In the case of calculations with BCS spectroscopic factors, we also included states in the continuum, but only for the $2f_{5/2}$, $1h_{9/2}$, and $1i_{13/2}$ configurations which, according to the KD potential, display low-lying resonances and hence might potentially affect the transfer cross sections.

In this calculation, the possibility of producing ^7Li in its ground and first excited states was considered. Furthermore, the possibility of ^8Li being in the ground state, first excited state and second excited state was taken into account. For this calculation, the spectroscopic factors presented in [3,21] were considered (see Table II).

The results of the CRC calculations are shown in Figs. 2 and 4. The solid and dashed red lines correspond to the region comprised by the two aforementioned calculations. In Fig. 4, it is observed that the ^7Li angular distribution at 25.8 MeV is very well reproduced by the CRC calculation, both in shape and magnitude.

The elastic angular distribution is also partially well reproduced, including the observed suppression of the Fresnel peak at forward angles. At backward angles, an underestimation of the experimental cross sections by the CDCC calculation is observed. The CRC calculation exhibits an increase with respect to the no-continuum calculation at these angles, which points to the importance of the one-neutron stripping channel in the backward angular region. It was found that the real normalization $N_r = 0.6$ used in the DF bare potential plays an importante role in the backward rise observed in the data. The same CRC calculations with $N_r = 1$ gave a smaller effect at backward angles.

E. The angle-integrated breakup cross sections

Because the IAV and CRC methods provide a good description of the ^7Li angular distributions, one can rely on the angle-integrated cross sections. In Table III we provide a comparison between the present total ^8Li breakup cross sections and those for the ^{120}Sn, ^{58}Ni, and ^9Be targets, obtained from previous CRC and IAV analyses [2,3]. The results can

FIG. 5. Coupled scheme of the $^{120}\text{Sn}(^8\text{Li}, ^7\text{Li})$ reaction for the CRC1 calculations. For the CRC2, the $2f_{5/2}$ state is in the continuum (see Table I for more details).

TABLE III. Total (angle integrated) breakup cross sections (σ_{bu}) and total reaction cross section for ^{8}Li on ^{9}Be [2], ^{58}Ni [3], and ^{120}Sn targets.

System	E_{lab} (MeV)	σ_{bu}^{CRC} (mb)	$\sigma_{bu}^{IAV+CDCC}$ (mb)	σ_{reac}^{OM} (mb)	σ_{reac}^{CRC} (mb)	$\sigma_{bu}/\sigma_{reac}$
^{8}Li + ^{9}Be	23.8		124(5)	1440		0.0861(35)
^{8}Li + ^{58}Ni	23.9	244	291	1194	1354	0.210(23)
^{8}Li + ^{58}Ni	26.1	242	290	1322	1484	0.190(20)
^{8}Li + ^{58}Ni	28.7	236	284	1446	1606	0.170(18)
^{8}Li + ^{58}Ni	30.0	233	281	1500	1657	0.163(17)
^{8}Li + ^{120}Sn	21.7	278.6(13)	274	348	533(11)	0.794(8)
^{8}Li + ^{120}Sn	25.8	308(7)	319	863	1028(30)	0.363(2)

be compared with the total reaction cross sections obtained from the OM and CRC analysis of the elastic scattering data. It is interesting to note that, in all cases, the $\sigma_{bu}/\sigma_{reac}$ ratio increases as E/V_b decreases, indicating that inclusive breakup processes (transfer/breakup) become relatively more important for lower reduced energies (see Table III). The results show that the total ^{7}Li production cross section increases from lighter to heavier targets, being 36%–79% for the ^{8}Li + ^{120}Sn system, around 15–20% for ^{58}Ni, and only 9% for the ^{9}Be target. The ratio between the total ^{7}Li production and the total reaction cross section increases as the reduced energy (E/V_b) decreases, indicating that the transfer/breakup process becomes relatively more important as the energy approaches the Coulomb barrier. Similar behavior has also been observed for other more exotic neutron-rich projectiles such as ^{6}He + ^{120}Sn [22,36], ^{11}Be [7], and ^{11}Li + ^{208}Pb [6] and also in the proton-rich case ^{8}B + ^{208}Pb, where the ratio reaches unity at energies below the Coulomb barrier [63].

IV. SUMMARY AND CONCLUSIONS

Particle distributions from the ^{8}Li + ^{120}Sn reaction was measured at laboratory energies of 21.7 and 25.8 MeV. The elastic scattering angular distribution exhibits a typical Fresnel pattern dominated by the Coulomb interaction, as expected for low-energy heavy-target collisions. These elastic distributions were compared with optical model, continuum-discretized coupled-channels and coupled reaction channels calculations. A clear reduction of the σ/σ_{Ruth} ratio was observed in the ^{8}Li + ^{120}Sn elastic distributions at forward angles, in an angular region around the expected position of the Fresnel peak. The comparison with the CDCC and CRC calculations indicates that CDCC partially accounts for this reduction, whereas the CRC provides a better agreement with the data at forward angles. In addition to the Fresnel peak reduction, an enhancement of the cross section ratio is observed at backward angles, which is not explained by the coupling with the breakup channel (CDCC calculations). On the other hand, the CRC calculations provide a very good explanation form the backward rise, indicating that this effect is due to the coupling with the neutron transfer channel.

In contrast to the results obtained previously for the same projectile on ^{9}Be and ^{58}Ni targets, the ^{7}Li energy distribution for ^{120}Sn shows a dominance of transfer to ^{121}Sn bound states over unbound states. The Q-value distribution of the ^{7}Li production channel at $E = 25.8$ MeV and the recoil nucleus excitation energy shows a maximum at high excitation energies, but it is still below the neutron threshold. The data were very well described by the calculations using the IAV inclusive breakup model, with no adjustable parameters. Due to low statistics, no ^{7}Li energy distribution was obtained at 21.7 MeV.

The ^{7}Li angular distributions have been well reproduced by both the IAV plus CDCC and CRC calculations at 25.8 MeV. The larger experimental errors for the lower incident energy prevent a detailed comparison with the theory, but the overall magnitude of the measured cross sections seems to be accounted for by both calculations without adjustable parameters. At both energies, the projectile elastic breakup contribution to the ^{7}Li yield is very small.

The angle-integrated ^{7}Li total breakup cross section was obtained from the IAV plus CDCC and CRC calculations and was compared with the total cross sections obtained previously for the ^{58}Ni and ^{9}Be targets. Both IAV+CDCC and CRC provide very similar total cross sections with a dominance of nonelastic breakup (including transfer to bound states) over elastic breakup. The results show that the total ^{7}Li production cross section increases from lighter to heavier targets and the ratio between the total ^{7}Li production and the total reaction cross section increases as the reduced energy (E/V_b) decreases, indicating that the inclusive breakup of the projectile becomes relatively more important as the energy approaches the Coulomb barrier. For the present ^{8}Li + ^{120}Sn data, this ratio is larger and the neutron transfer to bound states seems to be the dominant process for the ^{7}Li production, with a smaller contribution from the transfer to continuum.

[1] N. Keeley, N. Alamanos, K. Kemper, and K. Rusek, Elastic scattering and reactions of light exotic beams, Prog. Part. Nucl. Phys. **63**, 396 (2009).

[2] O. C. B. Santos, R. Lichtenthäler, A. M. Moro, K. C. C. Pires, U. Umbelino, A. S. Serra, E. O. N. Zevallo, A. L. de Lara, V. Scarduelli, J. Alcántara-Núñez, A. Lépine-Szily, J. Lei, S. Appannababu, and M. Assunção, One-neutron stripping from ^{8}Li projectiles to ^{9}Be target nuclei, Eur. Phys. J. A **59**, 48 (2023).

[3] O. C. B. Santos, R. Lichtenthäler, K. C. C. Pires, U. Umbelino, E. O. N. Zevallos, A. L. de Lara, A. S. Serra, V. Scarduelli, J. Alcántara-Núñez, V. Guimarães, A. Lépine-Szily, J. C. Zamora, A. M. Moro, S. Appannababu, M. Assunção, A. Barioni, R. Linares, V. A. B. Zagatto, P. N. de Faria, M. C. Morais *et al.*, Evidence of the effect of strong stripping channels on the dynamics of the ^{8}Li + ^{58}Ni reaction, Phys. Rev. C **103**, 064601 (2021).

[4] J. J. Kolata, V. Z. Goldberg, L. O. Lamm, M. G. Marino, C. J. O'Keeffe, G. Rogachev, E. F. Aguilera, H. García-Martínez, E. Martinez-Quiroz, P. Rosales, F. D. Becchetti, T. W. O'Donnell, D. A. Roberts, J. A. Brown, P. A. DeYoung, J. D. Hinnefeld, and S. A. Shaheen, Elastic scattering and transfer in the ^{8}Li + ^{208}Pb system near the Coulomb barrier, Phys. Rev. C **65**, 054616 (2002).

[5] A. Di Pietro, P. Figuera, F. Amorini, C. Angulo, G. Cardella, S. Cherubini, T. Davinson, D. Leanza, J. Lu, H. Mahmud, M. Milin, A. Musumarra, A. Ninane, M. Papa, M. G. Pellegriti, R. Raabe, F. Rizzo, C. Ruiz, A. C. Shotter, N. Soić *et al.*, Reactions induced by the halo nucleus ^{6}He at energies around the Coulomb barrier, Phys. Rev. C **69**, 044613 (2004).

[6] J. P. Fernández-García, M. Cubero, L. Acosta, M. Alcorta, M. A. G. Alvarez, M. J. G. Borge, L. Buchmann, C. A. Diget, H. A. Falou, B. Fulton, H. O. U. Fynbo, D. Galaviz, J. Gómez-Camacho, R. Kanungo, J. A. Lay, M. Madurga, I. Martel, A. M. Moro, I. Mukha, T. Nilsson *et al.*, Simultaneous analysis of the elastic scattering and breakup channel for the reaction ^{11}Li + ^{208}Pb at energies near the Coulomb barrier, Phys. Rev. C **92**, 044608 (2015).

[7] F. Duan, Y. Yang, K. Wang, A. Moro, V. Guimarães, D. Pang, J. Wang, Z. Sun, J. Lei, A. Di Pietro, X. Liu, G. Yang, J. Ma, P. Ma, S. Xu, Z. Bai, X. Sun, Q. Hu, J. Lou, X. Xu *et al.*, Scattering of the halo nucleus ^{11}Be from a lead target at 3.5 times the Coulomb barrier energy, Phys. Lett. B **811**, 135942 (2020).

[8] A. Di Pietro, G. Randisi, V. Scuderi, L. Acosta, F. Amorini, M. J. G. Borge, P. Figuera, M. Fisichella, L. M. Fraile, J. Gomez-Camacho, H. Jeppesen, M. Lattuada, I. Martel, M. Milin, A. Musumarra, M. Papa, M. G. Pellegriti, F. Perez-Bernal, R. Raabe, F. Rizzo *et al.*, Elastic scattering and reaction mechanisms of the halo nucleus ^{11}Be around the Coulomb barrier, Phys. Rev. Lett. **105**, 022701 (2010).

[9] E. F. Aguilera, P. Amador-Valenzuela, E. Martinez-Quiroz, D. Lizcano, P. Rosales, H. García-Martínez, and A. Gómez-Camacho, Near-barrier fusion of the ^{8}B + ^{58}Ni proton-halo system, Phys. Rev. Lett. **107**, 092701 (2011).

[10] K. Wang *et al.* (RIBLL Collaboration), Elastic scattering and breakup reactions of the proton drip-line nucleus ^{8}B on ^{208}Pb at 238 MeV, Phys. Rev. C **103**, 024606 (2021).

[11] L. Yang, C. J. Lin, H. Yamaguchi, A. M. Moro, N. R. Ma, D. X. Wang, K. J. Cook, M. Mazzocco, P. W. Wen, S. Hayakawa, J. S. Wang, Y. Y. Yang, G. L. Zhang, Z. Huang, A. Inoue, H. M. Jia, D. Kahl, A. Kim, M. S. Kwag, M. L. Commara *et al.*, Breakup of the proton halo nucleus ^{8}B near barrier energies, Nat. Commun. **13**, 7193 (2022).

[12] J. F. Liang, J. R. Beene, A. Galindo-Uribarri, J. Gomez del Campo, C. J. Gross, P. A. Hausladen, P. E. Mueller, D. Shapira, D. W. Stracener, R. L. Varner, J. D. Bierman, H. Esbensen, and Y. Larochelle, Breakup of ^{17}F on ^{208}Pb near the Coulomb barrier, Phys. Rev. C **67**, 044603 (2003).

[13] A. Barioni, V. Guimarães, A. Lépine-Szily, R. Lichtenthäler, D. R. Mendes, Jr., E. Crema, K. C. C. Pires, M. C. Morais, V. Morcelle, P. N. de Faria, R. P. Condori, A. M. Moro, D. S. Monteiro, J. M. B. Shorto, J. Lubian, and M. Assunção, Elastic scattering and total reaction cross sections for the ^{8}Li + ^{12}C system, Phys. Rev. C **80**, 034617 (2009).

[14] A. Pakou, N. Keeley, D. Pierroutsakou, M. Mazzocco, L. Acostaz, X. Aslanoglou, A. Boiano, C. Boiano, D. Carbone, M. Cavallaro, J. Grebosz, M. La Commara, C. Manea, G. Marquinez-Duran, I. Martel, C. Parascandolo, K. Rusek, A. M. Sánchez-Benítez, O. Sgouros, C. Signorini *et al.*, Important influence of single neutron stripping coupling on near-barrier ^{8}Li + ^{90}Zr quasi-elastic scattering, Eur. Phys. J. A **51**, 90 (2015).

[15] A. Pakou, D. Pierroutsakou, and M. Mazzocco, Total reaction cross sections for ^{8}Li + ^{90}Zr at near-barrier energies, Eur. Phys. J. A **51**, 55 (2015).

[16] O. Camargo, V. Guimarães, R. Lichtenthäler, V. Scarduelli, J. J. Kolata, C. A. Bertulani, H. Amro, F. D. Becchetti, H. Jiang, E. F. Aguilera, D. Lizcano, E. Martinez-Quiroz, and H. Garcia, ^{9}Be(^{8}Li, ^{9}Be)^{8}Li elastic-transfer reaction, Phys. Rev. C **78**, 034605 (2008).

[17] V. Guimarães, R. Lichtenthäler, O. Camargo, A. Barioni, M. Assunção, J. J. Kolata, H. Amro, F. D. Becchetti, H. Jiang, E. F. Aguilera, D. Lizcano, E. Martines-Quiroz, and H. Garcia, Neutron transfer reactions induced by ^{8}Li on ^{9}Be, Phys. Rev. C **75**, 054602 (2007).

[18] S. Mukherjee, N. N. Deshmukh, V. Guimarães, J. Lubian, P. R. S. Gomes, A. Barioni, S. Appannababu, C. C. Lopes, E. N. Cardozo, K. C. C. Pires, R. Lichtenthäler, A. Lépine-Szily, D. S. Monteiro, J. M. B. Shorto, P. N. de Faria, E. Crema, V. Morcelle, M. C. Morais, and R. Pampa Condori, Total reaction cross-sections for light weakly bound systems, Eur. Phys. J. A **45**, 23 (2010).

[19] F. D. Becchetti, W. Z. Liu, K. Ashktorab, J. F. Bajema, J. A. Brown, J. W. Jänecke, D. A. Roberts, J. J. Kolata, K. L. Lamkin, A. Morsad, R. J. Smith, X. J. Kong, and R. E. Warner, Systematics of ^{8}Li-induced radioactive beam reactions: $E = 13$–20 MeV, Phys. Rev. C **48**, 308 (1993).

[20] D. R. Mendes, A. Lépine-Szily, P. Descouvemont, R. Lichtenthäler, V. Guimarães, P. N. de Faria, A. Barioni, K. C. C. Pires, V. Morcelle, R. Pampa Condori, M. C. Morais, E. Leistenschneider, C. E. F. Lima, J. C. Zamora, J. A. Alcantara, V. Zagatto, M. Assunção, and J. M. B. Shorto, ^{8}Li$(p, \alpha)^5$He reaction at low energies, and ^{9}Be spectroscopy around the proton threshold, Phys. Rev. C **86**, 064321 (2012).

[21] A. M. Moro, R. Crespo, H. Garcia-Martinez, E. F. Aguilera, E. Martinez-Quiroz, J. Gomez-Camacho, and F. M. Nunes, Reaction mechanisms in the scattering of ^{8}Li on ^{208}Pb around the Coulomb barrier, Phys. Rev. C **68**, 034614 (2003).

[22] P. N. de Faria, R. Lichtenthäler, K. C. C. Pires, A. M. Moro, A. Lépine-Szily, V. Guimarães, D. R. Mendes, Jr., A. Arazi, A. Barioni, V. Morcelle, and M. C. Morais, α-particle production in ^{6}He + ^{120}Sn collisions, Phys. Rev. C **82**, 034602 (2010).

[23] K. C. C. Pires, R. Lichtenthäler, A. Lépine-Szily, and V. Morcelle, Total reaction cross section for the ^{6}He $+$ ^{9}Be system, Phys. Rev. C **90**, 027605 (2014).

[24] K. C. C. Pires, R. Lichtenthäler, A. Lépine-Szily, V. Guimarães, P. N. de Faria, A. Barioni, D. R. Mendes Junior, V. Morcelle, R. Pampa Condori, M. C. Morais, J. C. Zamora, E. Crema, A. M. Moro, M. Rodríguez-Gallardo, M. Assunção, J. M. B. Shorto, and S. Mukherjee, Experimental study of ^{6}He $+$ ^{9}Be elastic scattering at low energies, Phys. Rev. C **83**, 064603 (2011).

[25] S. Appannababu, R. Lichtenthäler, M. A. G. Alvarez, M. Rodríguez-Gallardo, A. Lépine-Szily, K. C. C. Pires, O. C. B. Santos, U. U. Silva, P. N. de Faria, V. Guimarães, E. O. N. Zevallos, V. Scarduelli, M. Assunção, J. M. B. Shorto, A. Barioni, J. Alcántara-Núñez, and V. Morcelle, Two-neutron transfer in the ^{6}He $+$ ^{120}Sn reaction, Phys. Rev. C **99**, 014601 (2019).

[26] K. Pfeiffer, E. Speth, and K. Bethge, Break-up of ^{6}Li and ^{7}Li on tin and nickel nuclei, Nucl. Phys. A **206**, 545 (1973).

[27] A. Pakou, N. Alamanos, A. Gillibert, M. Kokkoris, S. Kossionides, A. Lagoyannis, N. G. Nicolis, C. Papachristodoulou, D. Patiris, D. Pierroutsakou, E. C. Pollacco, and K. Rusek, α-particle production in the reaction ^{6}Li $+$ ^{28}Si at near-barrier energies, Phys. Rev. Lett. **90**, 202701 (2003).

[28] H. Kumawat, V. Jha, V. V. Parkar, B. J. Roy, S. Santra, V. Kumar, D. Dutta, P. Shukla, L. M. Pant, A. K. Mohanty, R. K. Choudhury, and S. Kailas, Inclusive α-production cross section for the ^{6}Li $+$ ^{90}Zr system at energies near the fusion barrier, Phys. Rev. C **81**, 054601 (2010).

[29] F. Souza, C. Beck, N. Carlin, N. Keeley, R. L. Neto, M. de Moura, M. Munhoz, M. Del Santo, A. Suaide, E. Szanto, and A. Szanto de Toledo, Reaction mechanisms in the ^{6}Li $+$ ^{59}Co system, Nucl. Phys. A **821**, 36 (2009).

[30] C. Signorini, M. Mazzocco, G. F. Prete, F. Soramel, L. Stroe, A. Andrighetto, I. J. Thompson, A. Vitturi, A. Brondi, M. Cinausero, D. Fabris, E. Fioretto, N. Gelli, J. Y. Guo, G. La Rana, Z. H. Liu, F. Lucarelli, R. Moro, G. Nebbia, M. Trotta *et al.*, Strong reaction channels at barrier energies in the system ^{6}Li $+$ ^{208}Pb, Eur. Phys. J. A **10**, 249 (2001).

[31] E. F. Aguilera, J. J. Kolata, F. M. Nunes, F. D. Becchetti, P. A. DeYoung, M. Goupell, V. Guimarães, B. Hughey, M. Y. Lee, D. Lizcano, E. Martinez-Quiroz, A. Nowlin, T. W. O'Donnell, G. F. Peaslee, D. Peterson, P. Santi, and R. White-Stevens, Transfer and/or breakup modes in the ^{6}He $+$ ^{209}Bi reaction near the Coulomb barrier, Phys. Rev. Lett. **84**, 5058 (2000).

[32] D. Brink, Kinematical effects in heavy-ion reactions, Phys. Lett. B **40**, 37 (1972).

[33] M. Ichimura, N. Austern, and C. M. Vincent, Equivalence of post and prior sum rules for inclusive breakup reactions, Phys. Rev. C **32**, 431 (1985).

[34] R. Lichtenthäler, A. Lépine-Szily, V. Guimarães, C. Perego, V. Placco, O. Camargo Jr., R. Denke, P. N. de Faria, E. A. Benjamim, N. Added, G. F. Lima, M. S. Hussein, J. Kolata, and A. Arazi, Radioactive ion beams in Brazil (RIBRAS), Eur. Phys. J. A **25**, 733 (2005).

[35] A. Lépine-Szily, R. Lichtenthäler, and V. Guimarães, The radioactive ion beams in Brazil (RIBRAS) facility, Eur. Phys. J. A **50**, 128 (2014).

[36] R. Lichtenthäler, O. C. B. Santos, A. Serra, U. Umbelino, K. C. C. Pires, J. R. B. Oliveira, A. Lépine-Szily, P. N. de Faria,

and V. Morcelle, Experiments with $A = 6$–8 exotic beams in RIBRAS, Eur. Phys. J. A **57**, 92 (2021).

[37] R. Lichtenthäler, M. A. G. Alvarez, A. Lépine-Szily, S. Appannababu, K. C. C. Pires, U. U. da Silva, V. Scarduelli, R. P. Condori, and N. Deshmukh, RIBRAS: The facility for exotic nuclei in Brazil, Few-Body Syst. **57**, 157 (2016).

[38] A. Lépine-Szily and R. Lichtenthäler, First results of the radioactive ion beam facility in Brasil (RIBRAS): Elastic scattering of ^{6}He and ^{8}Li beams on light and medium mass targets, Nucl. Phys. A **787**, 94 (2007).

[39] U. Umbelino, K. C. C. Pires, R. Lichtenthäler, V. Scarduelli, G. A. Scotton, A. Lépine-Szily, V. Guimarães, J. Lubian, B. Paes, J. L. Ferreira, M. A. G. Alvarez, J. M. B. Shorto, S. Appannababu, M. Assunçao, R. P. Condori, and V. Morcelle, Two-neutron transfer in ^{7}Be $+$ ^{9}Be collisions, Phys. Rev. C **99**, 064617 (2019).

[40] G. E. Knoll, *Radiation Detection and Measurement* (Wiley & Sons, New York, 1989).

[41] I. J. Thompson, Coupled reaction channels calculations in nuclear physics, Comput. Phys. Rep. **7**, 167 (1988).

[42] P. Descouvemont and E. C. Pinilla, Microscopic description of ^{8}Li $+$nucleus and of ^{8}B $+$nucleus scattering, Few-Body Syst. **60**, 11 (2019).

[43] G. R. Satchler and W. G. Love, Folding model potentials from realistic interactions for heavy-ion scattering, Phys. Rep. **55**, 183 (1979).

[44] M. F. Steeden, J. Coopersmith, S. J. Cartwright, M. D. Cohler, N. M. Clarke, and R. J. Griffiths, Phenomenological and microscopic optical potentials for 88 MeV ^{7}Li scattering, J. Phys. G: Nucl. Phys. **6**, 501 (1980).

[45] J. Cook, N. Clarke, and R. Griffiths, Optical-model analysis of ^{7}Li $+$ ^{25}Mg and ^{7}Li $+$ ^{27}Al elastic scattering at 89 MeV, Nucl. Phys. A **357**, 246 (1981).

[46] J. Cook, K. W. Kemper, and M. F. Vineyard, Description of large angle ^{6}Li $+$ ^{40}Ca scattering from 26 to 34 MeV using double-folded and $\alpha + d$ cluster potentials, Phys. Rev. C **26**, 486 (1982).

[47] Y. Sakuragi, M. Yahiro, and M. Kamimura, Chapter VI. Microscopic coupled-channels study of scattering and breakup of light heavy-ions, Prog. Theor. Phys. Suppl. **89**, 136 (1986).

[48] N. Keeley, S. Bennett, N. Clarke, B. Fulton, G. Tungate, P. Drumm, M. Nagarajan, and J. Lilley, Optical model analyses of ^{6,7}Li $+$ ^{208}Pb elastic scattering near the Coulomb barrier, Nucl. Phys. A **571**, 326 (1994).

[49] U. Umbelino, R. Lichtenthäler, O. C. B. Santos, K. C. C. Pires, A. S. Serra, V. Scarduelli, A. L. de Lara, E. O. N. Zevallos, J. C. Zamora, A. Lépine-Szily, J. M. B. Shorto, M. Assunçao, and V. A. B. Zagatto, Quasielastic scattering of light radioactive and stable projectiles on ^{9}Be, Phys. Rev. C **106**, 054602 (2022).

[50] N. Keeley, N. Alamanos, K. Rusek, and K. W. Kemper, Generation of a repulsive dynamic polarization potential by transfer couplings, Phys. Rev. C **71**, 014611 (2005).

[51] P. R. S. Gomes, J. Lubian, D. R. Otomar, T. Correa, R. Linares, L. F. Canto, and M. S. Hussein, Why the complete fusion of weakly bound nuclei is enhanced at sub-barrier energies and suppressed above the barrier? J. Phys.: Conf. Ser. **420**, 012121 (2013).

[52] M. Takashina, Y. Sakuragi, and Y. Iseri, Effect of halo structure on ^{11}Be $+$ ^{12}C elastic scattering, Eur. Phys. J. A **25**, 273 (2005).

[53] V. A. B. Zagatto, J. Lubian, L. R. Gasques, M. A. G. Alvarez, L. C. Chamon, J. R. B. Oliveira, J. A. Alcántara-Núñez, N. H.

Medina, V. Scarduelli, A. Freitas, I. Padron, E. S. Rossi, and J. M. B. Shorto, Elastic scattering, inelastic excitation, and neutron transfer for ^{7}Li + ^{120}Sn at energies around the Coulomb barrier, Phys. Rev. C **95**, 064614 (2017).

[54] A. Kundu, S. Santra, A. Pal, D. Chattopadhyay, R. Tripathi, B. J. Roy, T. N. Nag, B. K. Nayak, A. Saxena, and S. Kailas, Elastic, inelastic, and 1-nucleon transfer channels in the ^{7}Li + ^{120}Sn system, Phys. Rev. C **95**, 034615 (2017).

[55] A. J. Koning and J. P. Delaroche, Local and global nucleon optical models from 1 keV to 200 MeV, Nucl. Phys. A **713**, 231 (2003).

[56] J. Lei and A. M. Moro, Reexamining closed-form formulae for inclusive breakup: Application to deuteron- and ^{6}Li-induced reactions, Phys. Rev. C **92**, 044616 (2015).

[57] J. Lei and A. M. Moro, Numerical assessment of post-prior equivalence for inclusive breakup reactions, Phys. Rev. C **92**, 061602(R) (2015).

[58] G. Potel, F. M. Nunes, and I. J. Thompson, Establishing a theory for deuteron-induced surrogate reactions, Phys. Rev. C **92**, 034611 (2015).

[59] G. Potel, G. Perdikakis, B. V. Carlson, M. C. Atkinson, W. H. Dickhoff, J. E. Escher, M. S. Hussein, J. Lei, W. Li, A. O.

Macchiavelli, A. M. Moro, F. M. Nunes, S. D. Pain, and J. Rotureau, Toward a complete theory for predicting inclusive deuteron breakup away from stability, Eur. Phys. J. A **53**, 178 (2017).

[60] R. F. Carlton, S. Raman, J. A. Harvey, and G. G. Slaughter, Neutron transmission and capture gamma-ray measurements of ^{120}Sn + n, Phys. Rev. C **14**, 1439 (1976).

[61] G. Colò and X. Roca-Maza, HFBCS-QRPA code (unpublished), available from https://www0.mi.infn.it/~jroca/code/code.html, accessed 2024.

[62] G. Colò, L. Cao, N. Van Giai, and L. Capelli, Self-consistent RPA calculations with Skyrme-type interactions: The skyrme_rpa program, Comput. Phys. Commun. **184**, 142 (2013).

[63] A. Pakou, L. Acosta, P. D. O'Malley, S. Aguilar, E. F. Aguilera, M. Baines, D. Bardayan, F. D. Becchetti, C. Boomershine, M. Brodeur, F. Cappuzzello, S. Carmichael, L. Caves, E. Chávez, C. Flores-Vázquez, A. Gula, J. J. Kolata, D. Liu, D. J. Marín-Lámbarri, F. F. Morales *et al.*, Dominance of direct reaction channels at deep sub-barrier energies for weakly bound nuclei on heavy targets: The case ^{8}B + ^{208}Pb, Phys. Rev. C **102**, 031601(R) (2020).